JOURNAL OF MATERIALS SCIENCE **39** (2004) 7135–7143

Electrical and magnetic techniques for monitoring arc behaviour during VAR of INCONEL[1] 718: Results from different operating conditions

R. M. WARD, M. H. JACOBS
IRC in Materials Processing, University of Birmingham, Birmingham B15 2TT, UK
E-mail: r.m.ward@bham.ac.uk

Novel instrumentation and computer modelling are described which have been developed to detect and interpret current flows and magnetic fields during VAR. Results from different operating conditions during VAR of 20″ diameter ingots of INCONEL 718 at Special Metals Wiggin Ltd., Hereford are presented and discussed with reference to macrostructural findings. It is shown that the results support the viability of the measurement techniques, and that the techniques are capable of detecting subtle changes in arc behaviour. Freckles were formed under one set of experimental conditions, and it is shown that the distribution of the radial location of the arc centre (obtained from the magnetic field analysis) may help to explain this.

1. Introduction

Vacuum Arc Remelting (VAR) is used for the production of high quality nickel, titanium and iron-based alloys. Due to the stringent targets for the properties of these alloys in demanding applications, there is a continual drive to achieve further gains in the efficiency, capability and reproducibility of VAR. Techniques (such as numerical and analytical modelling) for reaching these goals require as much knowledge as possible concerning the process and the important quantities (e.g., heat, mass and current flows etc.) during operation. This paper focusses on the measurement of current flow and magnetic fields.

A number of VAR melts of 20 inch diameter INCONEL 718 have been instrumented at Special Metals Wiggin Ltd. (Hereford, UK), and two of these will be discussed here. Experimental measurements have been made of both the current flowing in the crucible and of the magnetic field surrounding it, and from these it is possible to deduce information concerning the arc processes inside the crucible. This information is extremely useful when determining appropriate boundary conditions for numerical models of the process, and also provides valuable insight into the process itself. Two areas of particular interest to numerical modellers include the amount of current that flows through the top and bottom of the ingot, and the radial distribution of current at the ingot top surface.

A 3d FE numerical model of current flow within VAR and the resulting magnetic field has been constructed using Opera-3d, and its use for interpreting the experimental data will be described. Data will be presented concerning the top/bottom current split under different conditions. The radial distribution of current flow at the ingot top surface is difficult to deduce quantitatively, but qualitative observations are possible and these will be presented, again under different conditions. Observations from material produced under these conditions will be discussed with reference to these results.

1.1. Current flows during VAR

Typical current flows during VAR are shown in Fig. 1, between the electrode, E, the ingot, I, the crucible sidewall, W, and the crucible base, B. It is important to note that although they are represented in the diagram as flows along a single line, in reality each of these currents has a spatial distribution.

Particular terms are used to describe different magnitudes and distributions of current flow during VAR. Often in response to changes in conditions such as arc gap, chamber pressure etc., a number of different kinds of arc behaviour can be observed and classified. For example Zanner and Bertram [1] describe diffuse and constricted arcs, drop shorts and glow. They write that the typically desired mode of arc operation is diffuse—given appropriate viewing hardware a fairly uniformly bright region can be seen over the surface of the ingot melt pool, often with several cathode spots visible as bright jets or spots extending from the underside of the electrode. In this condition, the heat and current transfer to the ingot are as widely and evenly spatially distributed as possible. A constricted arc occurs when, often under conditions of longer arc gap and/or higher chamber pressure, the arc shrinks down to approximately 1.5% of the area of the ingot top surface, providing a highly localised flux of metal, heat and current. A drop short describes a droplet of metal which

[1] INCONEL is a trademark of Special Metals.

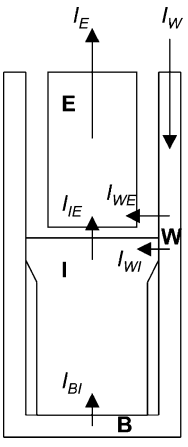

Figure 1 Current flows during VAR: I_E, Current from the electrode (= process current I_{total}); I_W, Current to the crucible wall (= I_{total}); I_{WE}, Current from the crucible wall to the electrode; I_{IE}, Current from the ingot to the electrode (= $I_{WI} + I_{BI}$); I_{WI}, Current from the crucible wall to the ingot; I_{BI}, Current from the crucible base to the ingot.

links the electrode and ingot, short circuiting the arc current temporarily until it breaks through ohmic heating and magnetic pinch forces. Glow describes a diffuse discharge in the region between the electrode and the crucible. Finally, current flow between the electrode and the crucible wall (rather than the ingot) is termed a side arc.

1.2. Possible influences of current flow

The distribution of current (and the corresponding induced magnetic fields) during VAR can affect the temperature and velocity distributions in the ingot melt pool. The most basic example of this is to consider a constricted arc situated at a point towards the edge of the melt pool, in which case the distribution of heat entering the melt pool would be strongly asymmetrical (with respect to the whole ingot).

Any induced JxB forces would then be similarly asymmetrical. Current flows during VAR are likely to play a role in the formation of macro- and microstructure, some of which may be cosmetic and some of which may be more serious. Current flows may also have an indirect influence; the likely effects of other defect processes (such as the fall-in and subsequent motion of crown material or electrode defects) will clearly depend upon the fluid motion and temperature fields in the molten pool, which are likely to be significantly affected by current flow. The relative magnitudes of the various current flows are also important. For example I_{WE} will tend to heat the crucible and the electrode sidewall, which may cause problems if too severe, whereas I_{IE} will heat the electrode bottom face and the ingot top surface, as desired.

2. Theoretical basis

It is extremely difficult to directly measure current flow during VAR because of the aggressive environment, so two indirect techniques are examined in this paper—the measurement of voltage gradients in the crucible wall, and the measurement of magnetic flux surrounding the crucible.

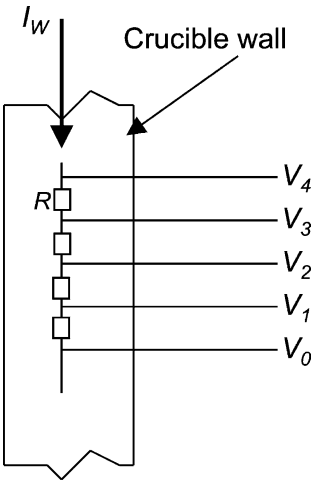

Figure 2 Voltage gradients in the VAR crucible wall.

The voltage gradient measurements are used to quantify the vertical distribution of current entering the ingot and electrode from the crucible wall. The magnetic flux measurements detect any deviations from axisymmetry in the current flow between the electrode and ingot. In conjunction with modelling they can be used to develop an understanding of the 3d current flows in VAR.

2.1. Voltage measurements

Current flow through the crucible will produce voltage gradients according to Ohm's law. Fig. 2 illustrates this—given a current I_W flowing through the equivalent circuit shown, $V_1 - V_0 = I_W * R$, $V_2 - V_0 = I_W * 2 * R$ etc. It is possible to calculate R from the electrical properties of copper, the crucible wall dimensions, and the measurement point spacing, allowing I_W to be determined from measurements of V_i. Typical values are estimated below:

$$J_W = \frac{I_W}{\pi\left(r_1^2 - r_0^2\right)}$$

$$\frac{\partial V}{\partial z} = \rho_e J_W$$

where, r_0, r_1 are the crucible wall inner and outer radii, ρ_e is the electrical resistivity of copper and z is the distance along the vertical axis. $I_W = 5800$ A, $r_1 = 0.267$ m, $r_0 = 0.255$ m and $\rho_e = 1.7 \times 10^{-8}\,\Omega$m, $J_W \approx 295$ kA/m^2 and $\partial V/\partial z \approx 5$ mV/m.

Hence over a typical measurement distance such as 5 cm the likely voltage differential would be approximately 250 μV. This is a small voltage to measure accurately in an electrically noisy environment, but it will be seen later that it is adequate to use as the basis for useful measurements.

It is important to note that the finite thickness of the crucible wall will lead to a 3 dimensional distribution of current flow in areas where current leaves the crucible wall, rather than the purely 1d (vertical) flow assumed in this analysis. This will probably lead to underestimates of current flow gradient over short vertical distances (e.g., less than the wall thickness) in which the current flow gradient is large.

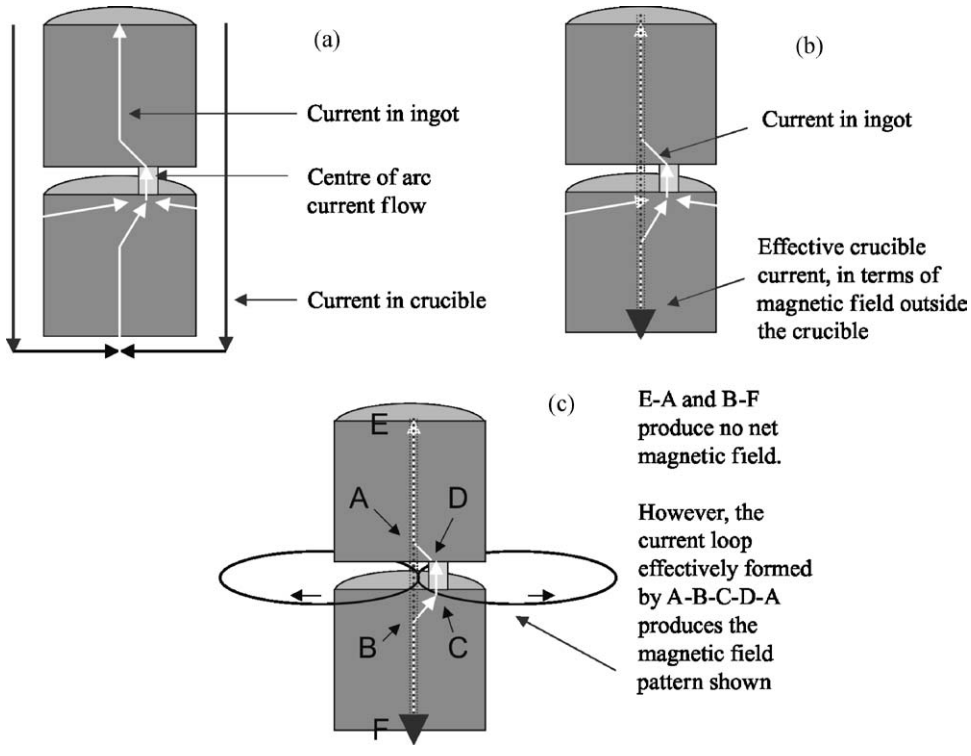

Figure 3 (a–c) Magnetic field resulting from off-centre current flow during VAR.

2.2. Magnetic field measurements

For the situation where the current flow through the crucible and its return through the ingot are both axisymmetric, it can be shown that the resultant magnetic field external to the crucible will be zero (consider Ampere's law on a circular path around the crucible). If either of these flows deviates from axisymmetry, however, an external field should be detectable. Such deviations are likely to be caused by drip shorts (as these are expected to be randomly distributed over the ingot top surface, and only to occur singly at any one time), by a constricted arc away from the ingot centreline, and even by a diffuse arc if is not perfectly centred. The likely shape of such a field is illustrated schematically (see Fig. 3).

An ideal measurement technique would be able to detect not only deviations from axisymmetry but also the radial distribution of even axisymmetric current flow. However it is difficult to conceive of a method for achieving this without putting sensors inside a VAR crucible.

The current flow and corresponding magnetic flux distributions under a number of different VAR conditions were modelled in 3-d using a finite element electromagnetic simulation package ('Opera 3d'). A number of factors were considered: Location of the centre of current flow between the electrode and ingot; Height of the contact zone between the ingot and crucible; Electrical resistance of the contact zone; Amount of current flowing to the ingot base. Examples of predictions of typical magnetic fields outside the crucible and current flows within the crucible are shown below (Figs 4–5 respectively).

The 3-dimensional magnetic field shown in Fig. 4 can be seen to be similar to that illustrated schematically in Fig. 3c. The predicted current flows are shown in Fig. 5. It can be seen that the current flowing in the crucible wall is predicted to concentrate at the same azimuthal angle as that of the arc from the ingot centreline (i.e., the crucible wall current wants to take the path of least resistance to get to the arc, and so concentrates in the crucible wall at the point closest to the arc). This local concentration will be significantly affected by the contact resistance between the ingot and crucible: if the contact resistance is high, then it will dominate the overall current flow and prevent any local concentration of current in the crucible wall.

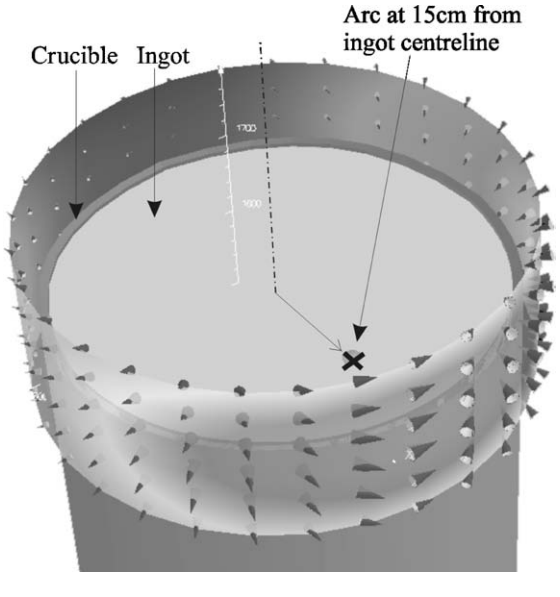

Figure 4 Magnetic fields around a VAR crucible, for an arc centre 15 cm from the ingot centreline.

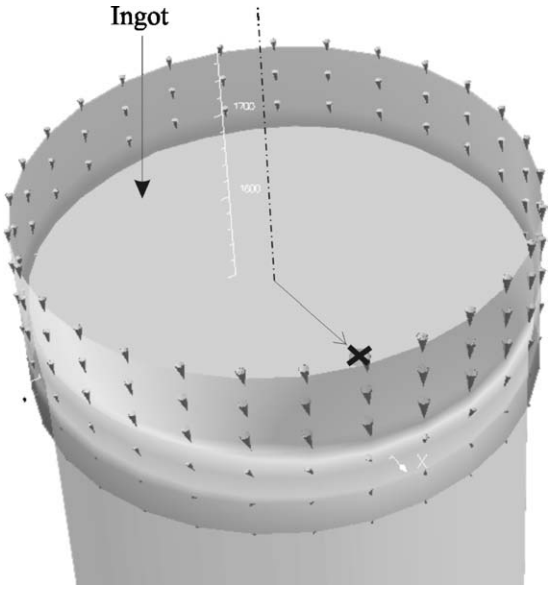

Figure 5 Current flow in the crucible wall during VAR, for an arc centre 15 cm from the ingot centreline.

3. Experimental method

Data gathered during VAR of 2 ingots of 0.5 m nominal diameter INCONEL 718 at Special Metals Wiggin Limited (Hereford, UK) will be presented here. The first ingot has already been reported on in [2] but is included here for comparison, and will be referred to as 'trial 1'. For the second ingot, two conditions were examined: 'trial 2a' and 'trial 2b'. The melt conditions are summarised (see Table I).

The magnetic flux densities were measured using circumferential bands of sensors. Twelve sensor boxes each containing either two or three sensors (measuring tangential, radial and axial flux density) were mounted around the crucible in a ring at a fixed distance above the crucible base, at 30° circumferentially from each other. The voltage outputs from the sensors were measured using a National Instruments differential amplifier and 10 KHz low pass filter. The crucible voltage gradients were measured by pairs of wires, each pair at 60° circumferentially from each other. As it was not possible to permanently modify the crucible, each wire was placed in electrical contact with the crucible using a small amount of electrically conductive paint and then secured with epoxy resin. The authors were aware that this might lead to galvanic and/or thermocouple effects, causing measurement errors. In each pair the bottom point was used as a voltage reference, and the voltage of the other wire was then measured differentially using a Nat. Inst. isolation amp. and 10 kHz low pass filter. This approach differs slightly from that taken by the authors of [3], who used absolute measurements of voltage relative to the crucible top with more widely vertically spaced sensors.

In trial 1 only a single band of sensors was used (detailed further in [2]). One band of sensors was used for each of trial 2a and 2b. The data acquisition details for trial 1 are listed in [2]. For trial 2 the power supply current and voltage were sampled at 25 kHz, and all other measurements at 5 kHz.

The ingot produced in trials 2a and 2b was sectioned transversely into sections about 30 cm tall. Each of these sections was cut longitudinally along the nominal ingot centreline, and a diametral slice taken from the front face of one side. Each of these slices was cut in two to give two half slices from the left and right sides of the melt pool. The left hand slices were macro-etched using acidic ferric chloride to reveal the grain structure. The right hand slices were electrolytically etched in 50% HCl, followed by an electrolytic stain in 4% H_2SO_4 to reveal segregation features. Variations in grain size were then visible on the left hand slices, whereas compositional defects such as freckles were most easily visible on the right hand slices.

TABLE I Experimental conditions

Condition	Mean current (A)	Arc gap	Melt rate (g/s)	Electrode diameter (mm)
Trial 1	5800	Normal	Normal 1	440
Trial 2a	6000	Decreased	Normal 2a	420
Trial 2b	6000	Increased	1.4 × (Normal 2a)	330

4. Results

Three types of result will be presented and discussed: (1) Crucible wall voltage gradients, (2) Magnetic flux density measurements outside the crucible, and (3) Macrostructural data.

4.1. Voltage gradient

It was shown in [2] that the effect of the temperature of the copper crucible wall on its resistivity needs to be considered if the measured voltage gradients are to be used to calculate current flows by Equation 1. That approach was followed here, and Fig. 6 shows the voltage measured between two wires mounted 5 cm apart on the crucible surface during trial 2a, and the temperature-corrected current flow calculated from it (averaged over 200 s). The gaps in the pale grey curve (crucible wall voltage) represent the intervals between successive data logs. Data to fill these gaps was created by linearly interpolating between the values at their endpoints. The current flowing in the crucible wall at the sensor location can be seen to fall from approximately 6000 to 0 A

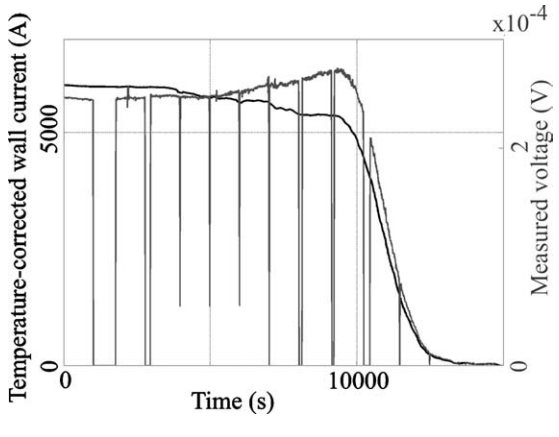

Figure 6 Voltage measured between two points on the crucible wall, and deduced temperature-corrected current flow.

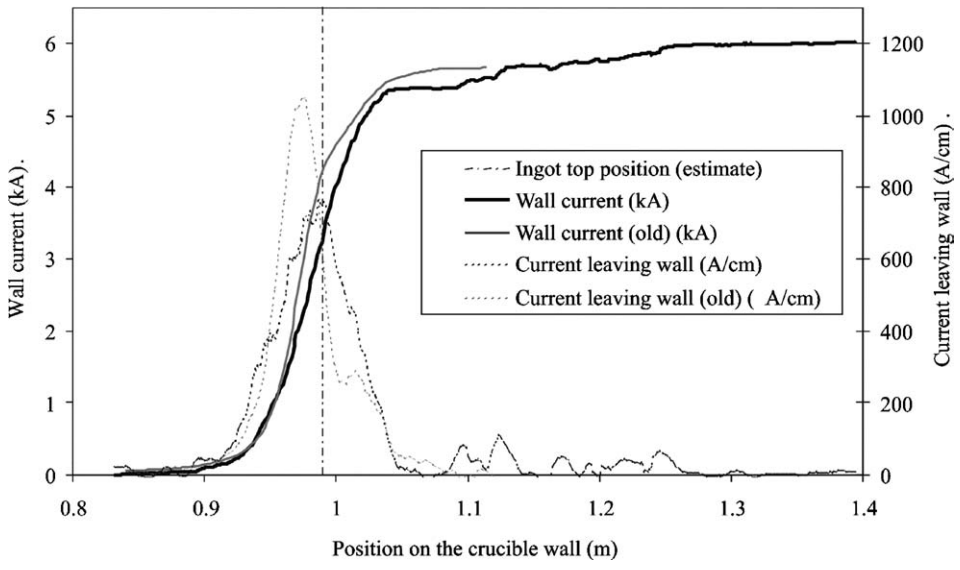

Figure 7 Crucible wall current above and below the ingot top position for trials 1 and 2a.

over about 12000 s (as the ingot top reached and passed the sensors).

As the VAR conditions were steady at this point it is acceptable to use this data as a measurement of the current flow at different places in the crucible wall relative to a fixed ingot top position (instead of as a measurement of current flow at a fixed wall position as the ingot top went past). Fig. 7 presents the data in this way, and shows both the crucible wall current (dark line) and its gradient with respect to crucible wall position (dark dashed line), as a function of crucible wall position for trial 2a. The data from trial 1 (for 5800 A, standard arc gap [2]) is also shown for comparison (pale lines).

The position of the ingot top was estimated as accurately as possible from the ingot weight, but an error band of $\pm$ 0.015 m should be applied. For trial 2a it can be seen that, at the ingot top position, approximately 3.3 kA was flowing in the crucible wall, thus $I_{WI} + I_{BI} =$ 3.3 kA. Taking into account the uncertainty in the ingot top position, an error of approximately $\pm$1000 A should be applied to this. As there was no measurable current flow at 20 cm below the ingot top, then $I_{BI} = 0$, and hence the current flowing into the top of the ingot from the crucible, $I_{WI} = 3.3(\pm 1)$ kA. Thus approximately $2.7(\pm 1)$ kA (= 6–3.3 kA) of current flows between the electrode and the crucible without entering the ingot at all, I_{WE}. It also follows that, as $I_{IE} = I_{WI} + I_{BI}$ and $I_{BI} = 0$, then $I_{IE} = I_{WI} = 3.3(\pm 1)$ kA.

In trial 2b the arc gap and melt rate varied during the experiment, which means that it is not possible to treat the data as time-invariant. In Fig. 8 therefore the wall current and rate of change of wall current are plotted as measured at the sensor, as a function of ingot top position, and thus appear to be inverted from left to right compared with Fig. 7. It is still possible to estimate the current flow to the ingot top and and electrode however, and in this case $I_{WI} = 4.4(\pm 0.8)$ kA and $I_{WE} = 1.6(\pm 0.8)$ kA . Again I_{BI} was found to be zero, subject to experimental error, so $I_{IE} = 4.4(\pm 0.8)$ kA .

4.2. Magnetic flux density

It is possible to use the model to estimate the magnetic flux density that should be measured at a sensor as the ingot top approaches from below and moves past. The problem for comparing this with measured data is that,

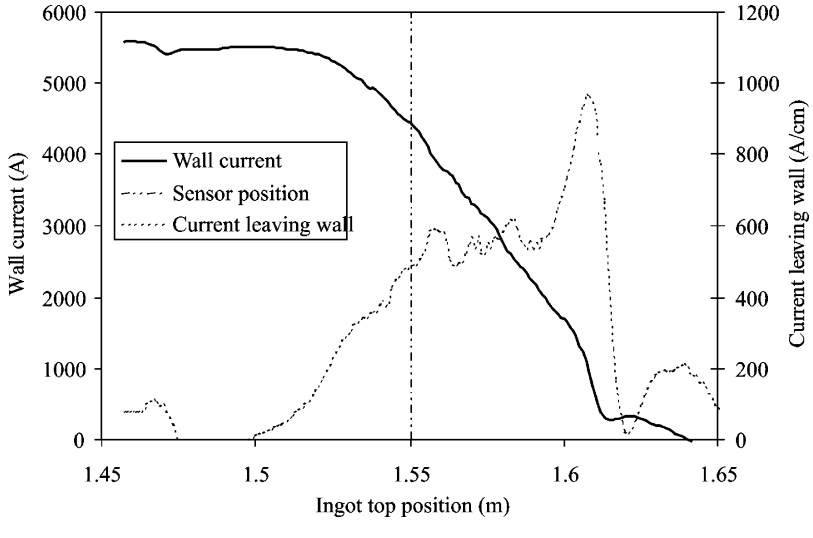

Figure 8 Crucible wall current measured at 1.55 mm during trial 2b, plotted as a function of ingot top position.

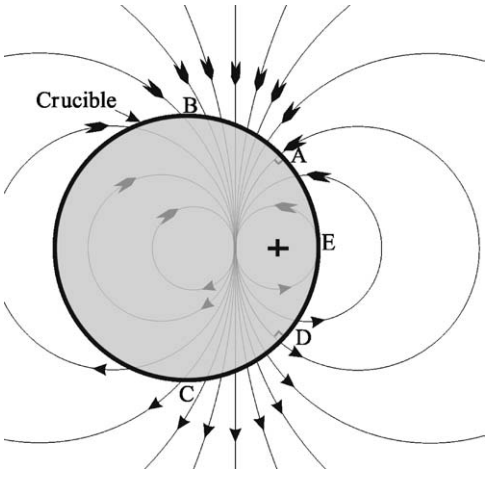

Figure 9 Schematic representation of the magnetic field surrounding a VAR furnace in which the effective electrical centre of the arc (represented by the cross) is displaced from the ingot centreline. The figure represents a horizontal section through the furnace, viewed from above.

at least initially, the position of the centre of the arc relative to the sensor is unknown. To combat this it is useful to assume that, over a sufficiently long time period (say 200 to 1000 s), the arc centre must have moved sufficiently for its position to be essentially random compared with the sensor. In this case statistics from the model computed in a complete circuit around the crucible can be compared with statistics from measurements at a single sensor. One example of this is to look at the distribution of measurements of radial and tangential magnetic flux density at a particular sensor.

A schematic representation of the magnetic flux pattern outside a VAR furnace resulting from an arc whose electrical centre is displaced from the ingot centreline is shown in Fig. 9, following the approach presented in Fig. 3. (The flux lines are drawn as continuing on inside the crucible (although dimmed) for clarity, although they are not correct there as the pattern inside the crucible would actually be dominated by the current from the arc itself). The flux lines enter and leave the crucible radially at points A and D, but at all other points there is also an azimuthal component to the flux.

At all points on the outside of the crucible along the sector ABCD, the azimuthal component of the flux is clockwise when viewed from above. At all points along the sector AED, however, the azimuthal component is anticlockwise from above, and the flux along this sector will be stronger as it is closer to the effective current paths. Thus the distribution of measurements of azimuthal magnetic flux, when averaged over time and over a number of sensors, would be expected to show a large number of clockwise values (along ABCD) and a smaller number of stronger, anticlockwise values (along AED). This can be observed in Fig. 10: most of the measured values of azimuthal flux (empty circles) are clockwise, but less than 2 in magnitude on an arbitrary scale, whereas the anticlockwise measurements are fewer in number, although stronger (down to as low as –9).

It can be seen from Fig. 9 that the radial component of flux, however, should be distributed symmetrically. For each point along DE with a strong outwards flux there is

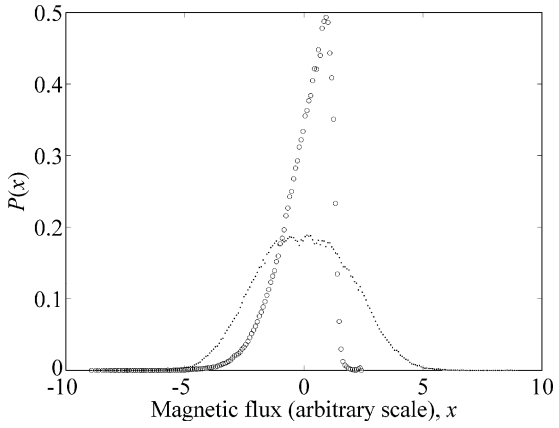

Figure 10 Distributions of magnetic flux measurements from the sensors outside the VAR crucible. The empty and filled circles represent the azimuthal and radial components respectively.

an equally strong inwards flux on AE, and similarly for the rest of the crucible. This can also be seen in Fig. 10: the distribution of measurements of radial magnetic flux (filled circles) is indeed symmetrical about 0.

Although it is useful to have overall statistics concerning predicted and observed arc behaviour, it is more valuable to be able to estimate the location of the effective centre of the arc at a given time. One method to achieve this is to compare the measured magnetic flux densities at a given time with a database of predicted values for different arc locations. Then the prediction which best matches the measured data can be found, and the arc location inferred. This approach was adopted here—simulations were performed for a number of radial arc locations, and software written to numerically interpolate between them as necessary. An optimisation routine was then used to estimate the location of the arc centre that gave the closest match between predicted and actual flux densities at the sensors. An example of this is presented below (Fig. 11), which shows a transverse section through the VAR crucible and sensor ring and in which the axes represent distance in mm. The

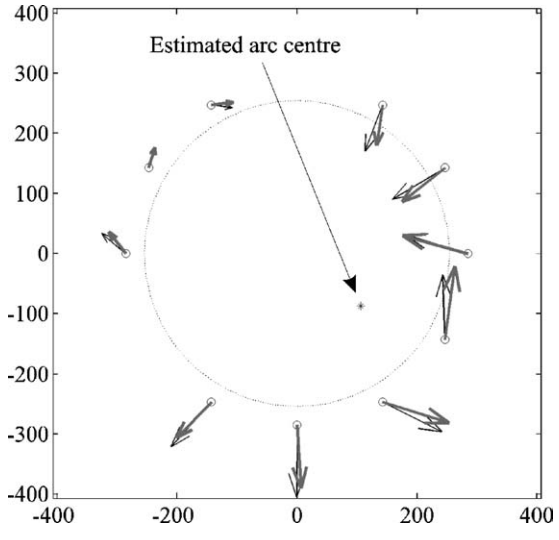

Figure 11 Measured and predicted values of magnetic flux density, for an arc centre estimated to be at the indicated point. Measured values are shown as solid black arrows, and values that were predicted from the estimated arc location are shown as grey arrows.

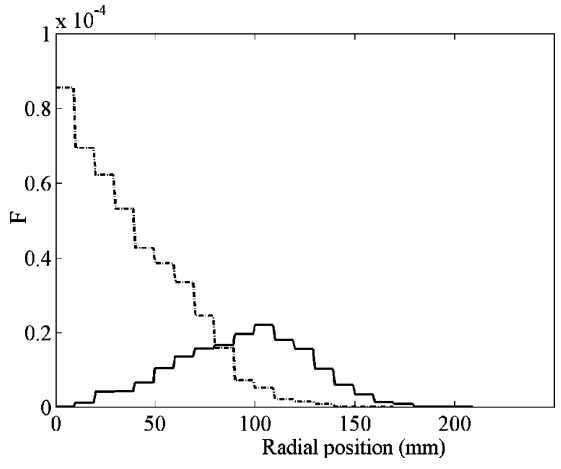

Figure 12 Distribution of position of the arc centre for normal electrode (420 mm diameter, solid line) and narrow electrode (330 mm diameter, dashed line). The frequency indicates the fraction of time that the arc centre was estimated to have spent per mm^2 area at a given radius, normalised so that $\int F(r) \cdot 2\pi r \cdot \mathrm{dr} = 1$.

data from only 10 magnetic flux density sensors was used in this analysis as it was found that two sensor boxes had malfunctioned. Therefore only 10 measurement points are shown in Fig. 11.

This analysis was undertaken over 50 s of data, sampling every 2 ms, to build up a time history of the estimated arc location. From the arc position history it was possible to calculate statistics such as, for a given radial distance from the ingot centreline, the fraction of time that a unit area at that location would expect to be under the arc centre. The results of such an analysis are shown (Fig. 12). If the arc were considered as a point source of current (which it is not), the lines on this graph would be proportional to the current input per mm^2 at the ingot top surface, as a function of distance from the ingot centreline.

4.3. Macrostructures

Grain-etched macrostructures from trial 2a and 2b are shown below (Fig. 13). Although difficult to see in this etched state, freckles are present as indicated in the macro from trial 2b.

It is useful to compare these results with those from a previous trial [4] in which the melting current was increased from approximately 6 to 7.5 kA during VAR of a 20″ diameter INCONEL 718 ingot. Although the melt rate increased by approximately 35% and the melt pool became deeper, no freckles were observed upon sectioning and etching the ingot.

5. Discussion

5.1. Voltage gradient measurements

Figs 7 and 8 illustrate how the current flowing at a given point in the crucible wall changed as the top of the ingot moved past. Before discussing the implications of these results it is important to consider aspects of the VAR process that might influence them. Fig. 1 showed an ingot top that was flat all the way across, with no crown. A probably more realistic situation is shown here (Fig. 14). In the analysis of the data undertaken here, the position of the ingot top was estimated from the ingot mass and the crucible dimensions. As the mass of the crown should be insignificant in comparison with that of the ingot, the 'estimated ingot top position' should be that of the top of the flat portion of the melt pool. In determining I_{WE} and I_{WI} it was assumed that all current leaving the crucible wall above the ingot top went to the electrode, and all current leaving below the ingot top went to the ingot. In reality it is likely that much of the current leaving the crucible wall in the 2–3 cm above the ingot top actually enters the ingot crown (I_{WC}). What is unknown is where it goes from there: If it goes into the electrode (I_{CE}) then the above assumptions are valid; If it goes into the

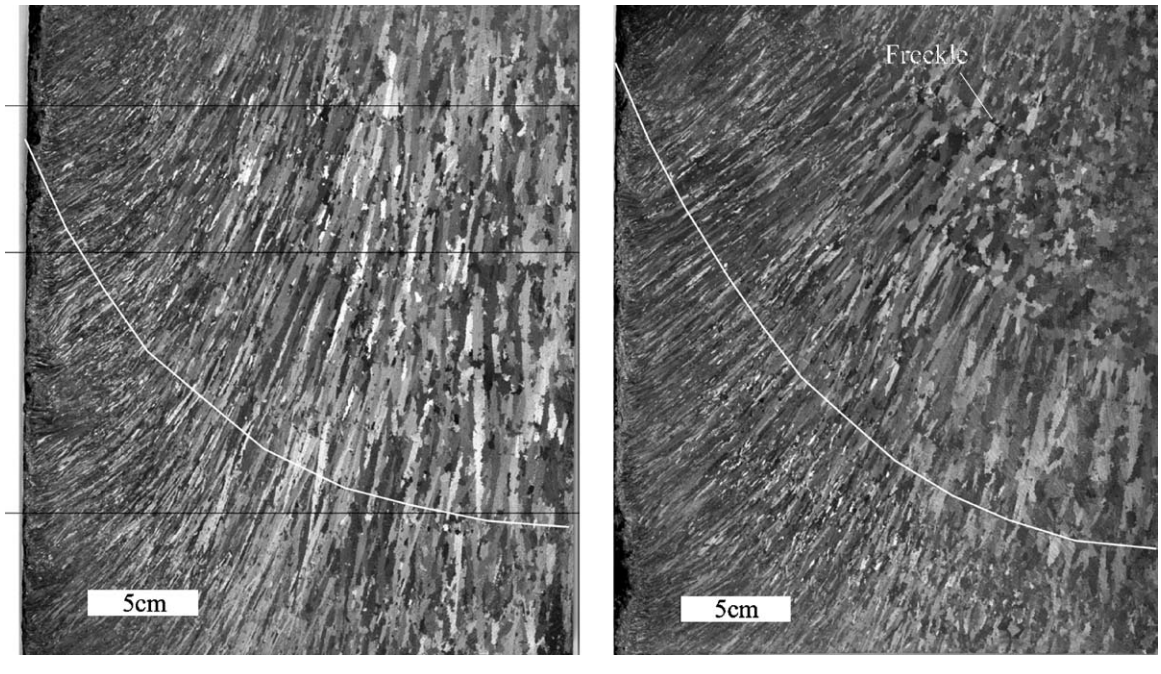

Figure 13 Grain-etch macros from trial 2a (left) and trial 2b (right), with melt pool shapes (estimated from macrostructural features) overlaid.

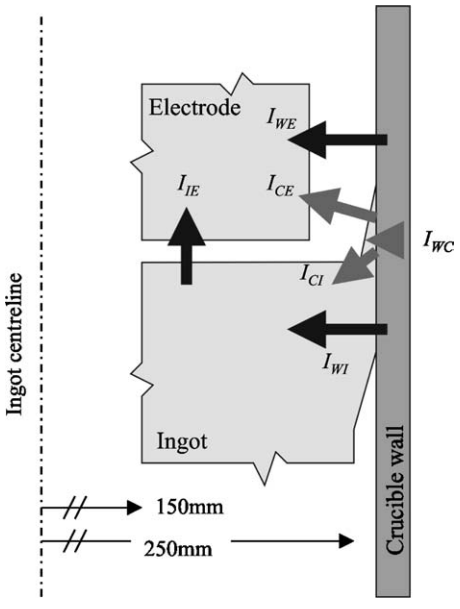

Figure 14 Possible current flows at the top of the ingot.

ingot (I_{CI}) then I_{WI} will have been underestimated, and I_{WE} overestimated. The implication from this is that, whatever happens in reality, I_{WI} should be equal to or greater than that estimated here.

In trial 2a I_{WI} was found to be 3.3 kA out of 6 kA I_{total}, implying that 55% of the applied current actually entered the ingot. (Assuming a 2 cm crown and that $I_{CE} = 0$, however, this could be increased to 4.5 kA or 75% I_{total}). It is interesting to note that the peak flow of current from the crucible wall to the ingot top ('Current leaving wall' in Fig. 7) is predicted to occur at the ingot top. In trial 1 I_{WI} was found to be 4.1 kA (70% I_{total}) under conditions similar to those of trial 2a. However the analysis of ingot top position used on the trial 1 data was not as sophisticated as that used for the data from trials 2a and 2b, and so it is possible that the estimated ingot top position in trial 1 is incorrect. If (as was found in trial 2a) the point at which maximum current leaves the crucible wall is used as the ingot top position in trial 1, then I_{WI} would be approximately 3.1 kA (or 53% of the 5800 A total current in that trial). In this case, the results from trial 1 and trial 2a would agree closely, in that 53 and 55% (plus any crown current) of I_{total} respectively would be estimated to enter the ingot.

As indicated in Table I, the electrode diameter was significantly reduced in trial 2b. In this trial I_{WI} was found to be 4.4 kA, 73% of I_{total}. The large increase in the current leaving the crucible wall at an ingot top position of approximately 1.61 m (Fig. 8) is thought to be the result of changing process parameters (not shown here) rather than an indication of the ingot top position.

Assuming this apparent increase in I_{WI} in trial 2b compared with trial 2a is not a measurement error, it is possible to speculate on a likely cause. As the distance from the electrode to the crucible wall in trial 2b (~90 mm) was approximately twice that of trial 2a (~45 mm), it is possible that this increased the electrical impedance experienced by current flowing from the crucible to the electrode, hence reducing I_{WE} and increasing I_{WI} (= I_{IE}).

It can be seen in Fig. 7 that the results for trial 2a suggest that current flowed between the crucible and electrode for at least 25 cm above the base of the electrode. Although possibly surprising, this is consistent with observations of arc tracks on aborted electrodes [5].

5.2. Magnetic flux density measurements

One of the main reasons for using a reduced diameter electrode in trial 2b was to validate the technique of collecting and interpreting the magnetic flux density sensor data to estimate the arc centre location. It was found in trial 2a and 2b that the effective electrical centre of the arc was estimated to be quite mobile rather than fixed in a particular location. This is a surprising result at first sight, but the results shown in Fig. 12 support the accuracy of this approach. The electrode used in trial 2a had a radius of 210 mm, and it can be seen that the distribution of measured arc centre locations for trial 2a extends as far as 200–210 mm. The electrode used in trial 2b had a radius of 165 mm, and it can be seen that the distribution of measured arc centre locations in this case extends as far as 160–170 mm.

The difference between the measured arc behaviours for the narrow electode (increased arc gap) and standard electrode (reduced arc gap) is striking. For the standard electrode, the arc centre was estimated to spend the greatest time per mm^2 at approximately 100–110 mm from the ingot centreline. (This does not mean that the arc centre was fixed at this radial location, but rather that, as it moved around the ingot surface, this was the most common.) For the narrow electrode however the arc centre was estimated to to spend the greatest time per mm^2 at the centre of the ingot. Further experimental work will be needed to determine which of the independent variables (arc gap and electrode diameter) had the greatest influence on the distribution of arc centre locations.

Unfortunately, due to the underlying physics, the time-averaged radial distribution of current entering the ingot top surface can not be inferred from the data presented here without an additional assumption regarding the shape of the current flow surrounding the arc centre at a given instant. Nonetheless, the marked difference in arc behaviour between trial 2a and 2b clearly indicates a significant difference between them, and a possible outcome of this will be discussed in Section 5.3.

5.3. Macrostructures

Although there are a number of differences between the macrostructures from trial 2a and 2b (Fig. 13), due to limitations of space only two aspects will be discussed here: melt pool shape, and the formation of freckles. The main differences between the operating conditions were (from Table I) that trial 2b was conducted with a melt rate approximately 40% higher than that of 2a, with a reduced electrode diameter, and with an increased arc gap. However rather than considering electrode diameter and arc gap directly, whose effects are hard to quantify, it is useful to consider the amount of current flowing between the

electrode and ingot, and the radial distribution of arc centre location.

The increased melt rate in trial 2b will have contributed significantly to its deeper melt pool, and probably to the formation of the freckles that were observed. The effects of the steeper angles of the solidus and liquidus fronts on freckle formation can be explored through freckle criteria such as those proposed and discussed in e.g., [6] and [7]. It is interesting to speculate, however, on whether the measured ingot current flow and the radial distribution of arc centre location also influenced both the melt pool shape and the freckle formation.

Assuming that the distribution of current flow follows in some way the distribution of arc centre location, then it would be expected (from Fig. 12) that the radial distribution of current flow at the ingot top surface in trial 2b was concentrated more closely towards the ingot centreline than that in trial 2a. This would create stronger Lorentz forces to drive flow downwards in the centre of the melt pool in trial 2b. The increased ingot/electrode current flow in trial 2b would also lead to stronger Lorentz forces. The estimated melt pool shapes in trial 2a and 2b are consistent with this hypothesis. It is also possible that stronger downward central flows would alter the temperature gradient ahead of the liquidus front and within the mushy zone, possibly encouraging freckle formation. As mentioned previously, no freckles were found in an earlier trial in which the melt rate had been increased by approximately 35% whilst keeping the arc gap and electrode diameter constant. Although this supports the hypothesis that arc phenomena (as well as melt rate) influence melt pool shape and defect formation, more work is needed to better understand this. It has been shown (e.g. [8]) that larger changes in arc current and melt rate are by themselves sufficient to cause freckle formation.

6. Conclusions

Techniques for measuring current flows and magnetic fields during VAR have been described, along with the use of computer modelling in interpreting them.

Depending on the effects of the crown, it is estimated that approximately 55–75% (±17%) of the total VAR current actually entered the ingot and flowed to the electrode under conditions close to those used industry-wide in production of 20″ diameter alloy 718 ingots. When a reduced diameter electrode and longer arc gap were used, however, then an increase to approximately 73–86%(±13%) was found. This change is consistent with the likely effects of reducing the electrode diameter (e.g., reduced electrode—crucible current flow).

It was found that the technique of using magnetic field measurements to deduce the location of the arc centre was strongly supported by the excellent match found to the diameter of the electrode sections used. The results obtained indicated dramatically different arc behaviour when the arc gap was increased and the electrode diameter reduced, consistent with (though not necessarily causative of) the production of freckles.

The approaches presented here should contribute to a better fundamental understanding of arc processes during VAR and their link to operating conditions. The data which can be obtained by using them should also reduce the uncertainties from unknown arc behaviour in modelling of VAR.

Acknowledgements

This work was supported through grant GR/N14163 from the UK EPSRC, and by Special Metals Wiggin Ltd., Rolls-Royce plc, Wyman Gordon and QinetiQ. Thanks to Brian Daniel, Richard Siddall, and Marlon Pritchard of Special Metals Wiggin for technical information and support, to Dave Evans of Special Metals and Peter Lee and Ahmad Kermanpur of Imperial College for discussion of boundary conditions, to Mike Glynn, Mark Barratt and Xianhui Wang of the IRC in Materials for help preparing for the experimental trials, to Dr. Fred Huang of the University of Birmingham for helpful discussion concerning the e/m field results, and to Frank Zanner for his encouragement.

References

1. F. J. ZANNER and L. A. BERTRAM, in Proc. 8th Int. Conf. Vac. Metall. (1985) p. 512.
2. R. M. WARD and M. H. JACOBS, in Proc. Int Symp. Liquid Metal Processing and Casting, Santa Fe NM 23-26/9/2001, edited by A. Mitchell and J. Van Den Avyle (American Vacuum Society, 2001) p. 244.
3. R. L. WILLIAMSON and G. J. SHELMIDINE, in Fifth International Symposium on Superalloys 718, 625, 706 and Derivatives, Pittsburgh, June 17–20, 2001, (TMS, 2001) p. 91.
4. R. M. WARD, X. XU, P. D. LEE, M. MCLEAN and M. H. JACOBS, in Proc. Int Symp. Liquid Metal Processing and Casting, Santa Fe NM 23-26/9/2001, edited by A. Mitchell and J. Van Den Avyle (American Vacuum Society, 2001) p. 187.
5. R. J. SIDDALL, Private Communication at Special Metals Wiggin Ltd., 2003.
6. P. AUBURTIN, S. L. COCKCROFT, A. MITCHELL and T. WANG, in Proc. Superalloys 2000, edited by T. M. Pollock *et al.* (TMS, 2000) p. 255.
7. W. YANG, W. CHEN, K. M. CHANG, K. MORITA, S. MANNAN, J. DEBARBADILLO and S. PATEL, in Proc. Int Symp. Liquid Metal Processing and Casting, Santa Fe NM 23–26/9/2001, edited by A. Mitchell and J. Van Den Avyle (American Vacuum Society, 2001) p. 314.
8. T. SUZUKI, T. SHIBATA, K. MORITA, T. TAKETSURU, D. G. EVANS and W. YANG, in Proc. Int Symp. Liquid Metal Processing and Casting, Santa Fe NM 23-26/9/2001, edited by A. Mitchell and J. Van Den Avyle (American Vacuum Society, 2001) p. 325.

Received 10 March
and accepted 25 June 2004